# Investigation on the Influence of Particle Size and Concentration on the Spray and Combustion Characteristics of Aluminium Particle Containing Gels with an Impinging Jet Injector

*K. Madlener, C. Sinatra[*] and H.K. Ciezki*
*DLR – German Aerospace Center*
*Institute of Space Propulsion*
*Lampoldshausen, Langer Grund, D-74239 Hardthausen, Germany*

## Abstract

The performance characteristics of various aluminized gelled fuels were determined in a detailed investigation concerning their rheological, spray and combustion properties. The viscosity properties were obtained for gels with different grades of Al particles with Sauter diameters in the range between 0.76 µm and 190 µm. For the determination of the atomization characteristics with a doublet like-on-like impinging jet injector setup 4 particle grades were selected. The results show that the curves for the Sauter diameters of the droplets in dependence of the jet velocity are in a similar range, whereas the measured diameters decrease with increasing gel jet velocity. The combustion characteristics of a selected gel in a combustion chamber under ramjet relevant conditions at 6 and 11 bar were obtained. They show higher efficiencies at the higher combustor pressure level and in general increasing efficiencies with increasing jet exit velocities.

## 1. Introduction

In the last years the improvement of specific impulses and flight distances are not anymore the only main research and development objectives for rocket and ramjet propulsion systems. Other properties like throttleability, simple handling and storage characteristics, higher safety levels, environmental aspects, etc. come more and more into focus. Gelled fuels and propellants offer the possibility to fulfill a significant number of demands of the above mentioned and desired system properties. Due to their shear-thinning non-Newtonian flow behavior they combine advantages of engines with liquid fuels (e.g. throttleability) and of engines with solid fuels (e.g. simple handling and storage characteristics).[1-3] Without any applied shear stress gelled fuels and propellants are in general non-capable of flow. Applying high shear rates, however, it is possible to reach relative low viscosity values so that an atomization similar to conventional liquid fuels is possible under distinct conditions as previous investigations have shown, see e.g. Refs. [4, 5].

In order to increase flight performances, the addition of metal particles like aluminium or boron, is of special interest due to their significantly higher energy content per unit volume in comparison to the pure hydrocarbon fuels. Slurry fuels, where metal particles are added to liquid hydrocarbon fuels, have yet been investigated in the past decades in detail, see e.g. Refs. [6-8]. Unfortunately this fuel type shows several severe problems in connection with long-time stability and stability under elevated accelerations due to sedimentation effects, etc., which have not yet been completely resolved.

In gelled fuels with metal particle addition, however, particle sedimentation effects are significantly lower than in slurries and separation effects occur only at very high acceleration levels. Up to now the knowledge level about the spray and combustion characteristics of metallized gel fuels is still relatively low.[2,9,10] An investigation concerning spray and combustion characteristics with only one aluminium particle grade with an average particle diameter of ca. 10 µm was conducted by von Kampen et al[4] and presented at the first EUCASS symposium in 2005 in Moscow. Due to the fact that their results are fixed on the one used particle grade, a better understanding concerning the influence of various particle phase parameters like average diameter, particle loading, diameter distribution, etc. on gel propulsion properties is necessary.

[*] Diploma degree student from SP Lab, Politecnico di Milano, Milan, Italy

Copyright © 2007 by the authors. Published by the EUCASS association with permission.

The present publication presents an investigation with various commercially available Al particle grades and shows the influence of particle size and particle phase concentration on spray and combustion characteristics of metallized gel fuels as well as on their rheological properties. For this task aluminium powders of different sizes were added to a basic gel fuel system based on Jet A-1, whose rheological and atomization characteristics are known.[10] It has to be mentioned in this context that the rheological properties have to be measured first, because viscosity characteristics must be known for the determination of boundary conditions of the spray and combustion experiments to be conducted. Furthermore, rheological measurements serve as a decision criterion, whether the produced gels would be sufficiently feedable in spray and combustion experiments.

## 2. Experimental Setup

### 2.1 Gel production and rheology

The gelled fuels were produced making use of a Getzmann dissolver stirrer apparatus. Jet A-1 was chosen for the presented experiments as basic fuel, because it is a commercially and easily available liquid fuel. It was gelled with Thixatrol ST, an organic-based gellant. Thixatrol ST is a castor oil derivative from Rheox, which was used together with 5-Methyl-2-Hexanone (Miak) for the vehicle/solvent mixture for the gellation process. All gels presented here were produced with constant amounts of 7.5 wt.-% Thixatrol ST and 7.5 wt.-% Miak, so that for the Al content variation also the Jet A-1 content was changed. For the rheological measurements, which were conducted as the first test series, the Al mass fraction $Y_{Al}$ was varied between 10 and 40 wt.-% for all particle grades. Table 1 gives an overview about the technical data of the used Al particle grades, which are commercially available. The average particle diameters are given both as $D_{50}$ (50 % of the particles are smaller than $D_{50}$) and the Sauter diameter $D_{3,2}$. For the particle grades from Ecka Granules these data have been obtained from particle distribution histograms delivered from the company. For the other grades (except PG3) the data have been determined from Malvern particle sizer measurements at the Fraunhofer Institute for Chemical Technology. Furthermore the slenderness ratio s of the histogram is given, which is defined as the ratio of the Sauter diameter to the diameter width Δd in the histogram between $D_5$ and $D_{95}$. The two diameters $D_5$ and $D_{95}$ are defined as the particle diameters, where 5% of the particles are smaller than $D_5$ and 95% are smaller than $D_{95}$.

Table 1: Particle grades

| No. | manufacturer | identification | Average Diameter $D_{50}$ [µm] | Average Diameter $D_{3,2}$ [µm] | Purity [% ] | $s=D_{3,2}/\Delta d$ |
|---|---|---|---|---|---|---|
| PG1 | Ecka Granules | MEP027 (1.5 µm) | 1.22 | 0.76 | 99.7 | 0.287 |
| PG2 | Ecka Granules | MEP103 (<10 µm) | 4.48 | 3.42 | 99.5 | 0.261 |
| PG3 | Alpha Aesar | A.A. <44 | 9.8 | | 99.8 | |
| PG4 | Ecka Granules | AS081 (<45 µm) | 25.21 | 19.83 | 99.5 | 0.441 |
| PG5 | Sigma Aldrich | S.A. <75 | 35.97 | 29.61 | 99 | 1.056 |
| PG6 | Ecka Granules | AS51 (<100 µm) | 45.49 | 33,43 | 99.5 | 0.304 |
| PG7 | Alpha Aesar | A.A. 44-149 | 94.47 | 84.75 | 99.5 | 0.841 |
| PG8 | Chempur | 009000 (<250 µm) | 157.3 | 127.4 | n.a. | 0.645 |
| PG9 | Alpha Aesar | A.A. 44-420 | 239.4 | 190 | 99.5 | 0.701 |

The rheological properties were obtained with a ThermoHaake RheoStress 1 rotational rheometer up to shear rates of approximately $\dot{\gamma}=10^4\ s^{-1}$, whereas the plate-plate geometry with a gap of 0.5 mm was used. For the non-aluminized gel a Rosand RH2000 capillary rheometer was used additionally to determine the viscosity characteristic up to shear rates $\dot{\gamma}=10^6\ s^{-1}$. Due to the danger of plugging, which could damage the capillary rheometer, measurements were not conducted for the aluminized gels.

### 2.2 Experimental setup for atomization investigations

The experimental set-up for the spray investigations is shown in the sketch of Fig. 1. The gelled fuel is stored in a cartridge and is fed to the injector unit by moving a piston inside the cartridge with a remote controlled hydraulic

driving unit and pushing the gel with a pre-selected volume flow rate through a pipe, which connects the cartridge with the injector unit. The pressure inside the cartridge and in the injector unit is monitored by pressure gauges.
For the spray investigation presented here, a doublet like-on-like impinging jet atomizer set-up was chosen. This injector type is often used in liquid rocket engines operated with storable Newtonian fuels due to its simplicity and its good atomization and mixing characteristics.[11] The modular injector set-up allows easy variation of impingement angle, impingement distance and injector exit diameter. All experiments presented in this publication were conducted with the same injector exit diameter $D = 0.7$ mm and an impingement angle between the two jets of $2\theta = 90°$. The shadowgraph technique was applied for the visualization of the spray behavior together with Xenon flash lights with a flash duration of 150 ns (FWHM) and CCD cameras with a maximum resolution of 1024x1024 pixel. The two shadowgraphy systems are perpendicular oriented so that the atomization behavior can be observed from two sides. Further information about the set-up and the injector design is given in Ref. [12].
Droplet size distributions within the spray were determined with Fraunhofer diffraction making use of a Malvern Spraytec, whereas the laser beam was oriented perpendicular to the fluid sheet plane. The instrument was aligned and calibrated using a reference reticle with known etched particle distributions. The droplet diameter measuring range of the setup is between 0.5 µm and 850 µm. The data acquisition rate was 500 Hz at a duration of 2 s.

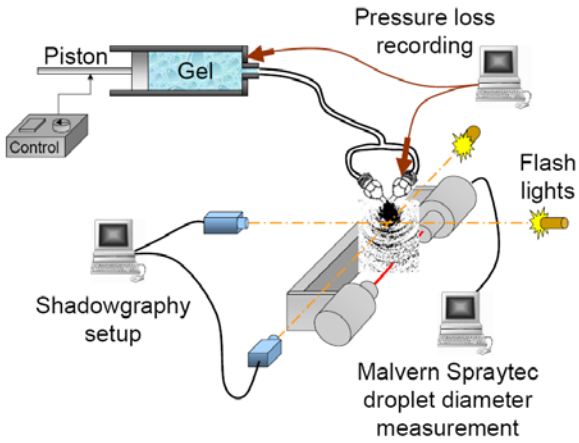


Figure 1: Experimental setup for spray investigations

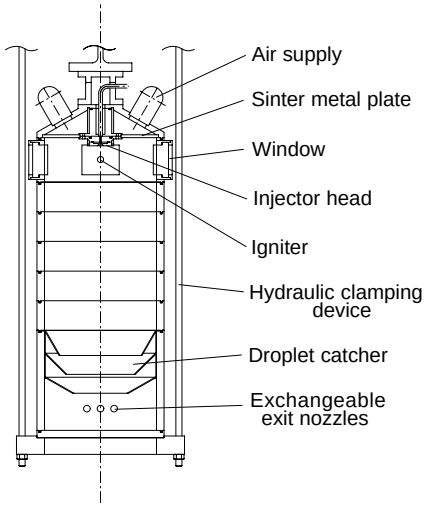


Figure 2: Sketch of the combustion chamber

## 2.3 Experimental setup for combustion investigations

For the investigation of the combustion characteristic of gelled fuels at conditions (pressure and air inlet temperature) relevant for ramjet application, a pressurized combustion chamber was used. This experimental setup, whose sketch is presented in Fig. 2, was designed for maximum combustor pressures of 12 bar and maximum air inlet temperatures of 800 K so that conditions up to flight Mach numbers of 3.5 at heights between approx. 15 to 30 km can be simulated (if isentropic air intake conditions are assumed). The combustion chamber has a diameter of 0.3 m, a height of 0.9 m and consists of steel rings, which are hold together by a hydraulic clamping device. The upper steel ring contains windows with quartz slices to provide a direct access of optical diagnostic tools to the occurring processes inside the chamber.
A hydrogen/oxygen ($H_2/O_2$) burner is used to ignite the gel spray. The pressure in the chamber can be varied by changing exit nozzles of different diameters, which are located in the lowest chamber ring. The injector head is mounted vertically to introduce the spray in a slowly vertically flowing hot air flow. A stainless steel sinter metal plate serves for homogenization of the air flow, which is heated by $H_2/O_2$ burners in a separate set-up (vitiated air). Exchangeable injector plates allow a quick variation of injection geometries.
For the combustion tests in the present investigation, the same injector geometry as in the spray investigations was used ($D = 0.7$ mm, $2\theta = 90°$). Experiments were conducted at 6 and 11 bar with three different temperatures of the incoming air: 300, 550 and 800 K. The gel jet exit velocity $\bar{u}$ was varied in four steps between 30 m/s and 60 m/s. An equivalence ratio $\phi = 0.23$ was chosen, which limits the thermal loads on the chamber walls and allows a largely undisturbed observation of the combustion process of the single impinging jet injector element.

## 3. Results and discussion

### 3.1 Rheological characteristics

Figure 3 shows the shear-thinning behavior of gels with the Al particle grade PG2, which has an average particle diameter $D_{3,2}$=3.42 µm. The 5 traces represent 5 different particle loadings (including the non-aluminized gel) with mass fractions $Y_{Al}$ = 0 %, 10 %, 20 %, 30 % and 40 %. It can be seen that for all traces decreasing shear viscosity values occur with increasing shear rates. Furthermore, the viscosity increases with increasing Al content. The measurements for the particle-loaded gels were conducted for shear rates up to ca. $\dot{\gamma} = 10^4$ s$^{-1}$. For higher shear rates up to $\dot{\gamma} = 10^6$ s$^{-1}$ measurements had to be conducted with a capillary rheometer using very small capillary orifices. Data in that shear rate range are only available for the non-aluminized gel because due to the danger of plugging the capillary rheometer was not used for the aluminized gels. The in earlier publications (see e.g. Refs. [10, 13, 15]) presented upper Newtonian plateau with its constant viscosity could therefore only be determined for the non-aluminized gel.

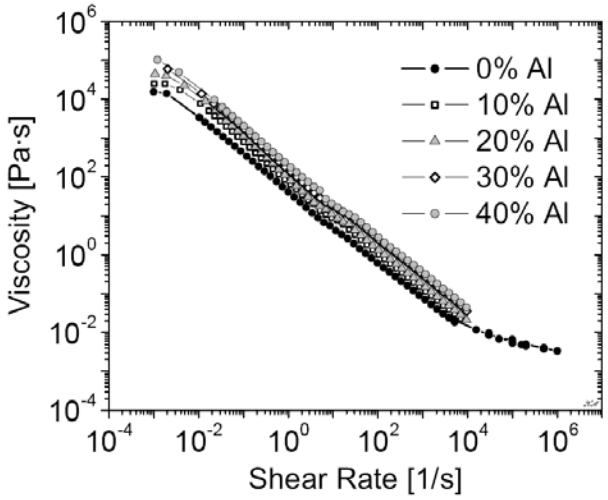


Figure 3: Dynamic shear viscosity versus shear rate for gels with the Al particle grade PG2 (Ecka, $D_{3,2}$ = 3.42 µm) with the Al mass fraction $Y_{Al}$ as additional parameter.

The viscosity characteristics of the investigated gels can theoretically be approached over the entire relevant shear rate range of $10^{-2}$ s$^{-1}$ < $\dot{\gamma}$ <$10^6$ s$^{-1}$ with the **H**erschel-**B**ulkley-**E**xtended equation (HBE). The HBE-equation, presented in Eq. 1, was introduced by Madlener & Ciezki[13] as an extended version of the Herschel-Bulkley law with an additional constant viscosity parameter $\eta_\infty$ for the high shear rate range.

$$\eta = \frac{\tau_0}{\dot{\gamma}} + K \cdot \dot{\gamma}^{n-1} + \eta_\infty \qquad (1)$$

In this equation $\tau_0$ [Pa] is the yield stress, $K$ [Pa·s$^n$] the pre-exponential factor, $n$ [-] the exponent and $\eta_\infty$ [Pa·s] the constant viscosity value for high shear rates. For the non-aluminized gel the viscosity could be determined in the high shear rate range, the asymptotic viscosity was determined to $\eta_\infty$ = 0.0036 Pa·s. For the particle-loaded gels, where capillary measurements were not conducted, assumptions had to be made for the values of $\eta_\infty$. The corresponding values for the gels with $Y_{AL}$ = 10 %, 20 %, 30 % and 40 % are $\eta_\infty$ = 0.0037 Pa·s, 0.0038 Pa·s, 0.004 Pa·s and 0.0042 Pa·s. The yield stress $\tau_0$ and the parameters $K$ and $n$ were determined by a mathematical approach to the shear rate dependent viscosity distribution.

Figure 4 presents the determined yield stress values $\tau_0$ in dependence of the Al mass fraction $Y_{Al}$ for gels with different aluminium particle grades. For a better presentation, the gels containing aluminium particles from Ecka Granules are summarized in the left diagram (PG1, PG2, PG4, PG6). The gels containing particles from Alpha Aesar and Sigma Aldrich (PG3, PG5, PG7) are presented in the right graph. The viscosity measurements of the gels with the Chempur particles PG8 and the Alpha Aesar particles PG9 are not presented here. The obtained results seemed not to be realistic, caused by the too large particle diameters for the available rheometer sensor geometries.

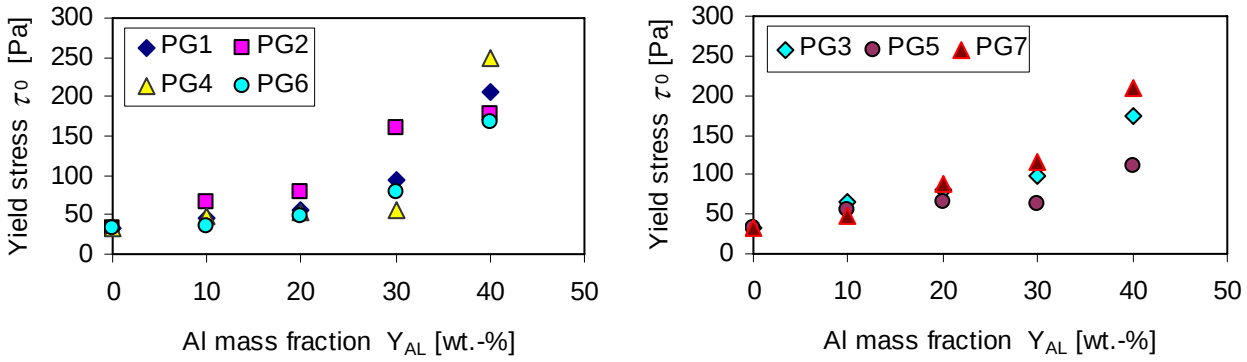


Figure 4: Yield stress $\tau_0$ versus the Al mass fraction $Y_{Al}$ for gels with various Aluminium particle grades.

Both diagrams of Fig. 4 show that with increasing aluminium content increasing yield stresses occur, whereas the gradient of the increase becomes generally steeper with increasing $Y_{Al}$. Figure 5 shows the dependence of the pre-exponential factor *K* from the Al mass fraction $Y_{Al}$ for gels with various Aluminium particle grades. *K* increases for increasing $Y_{Al}$ for almost all particle grades. It can be seen also in these diagrams that the slopes of the curves become irregular at high $Y_{Al}$, which is caused by measurement difficulties at high particle loadings. Figure 6 presents the exponential factor *n* of the HBE-equation in dependence of the aluminium mass fraction. For low particle loadings, the value of the exponent is mostly near n = 0.2. At higher loadings the measured values show stronger deviations from this value with no clear tendency towards increase or decrease.

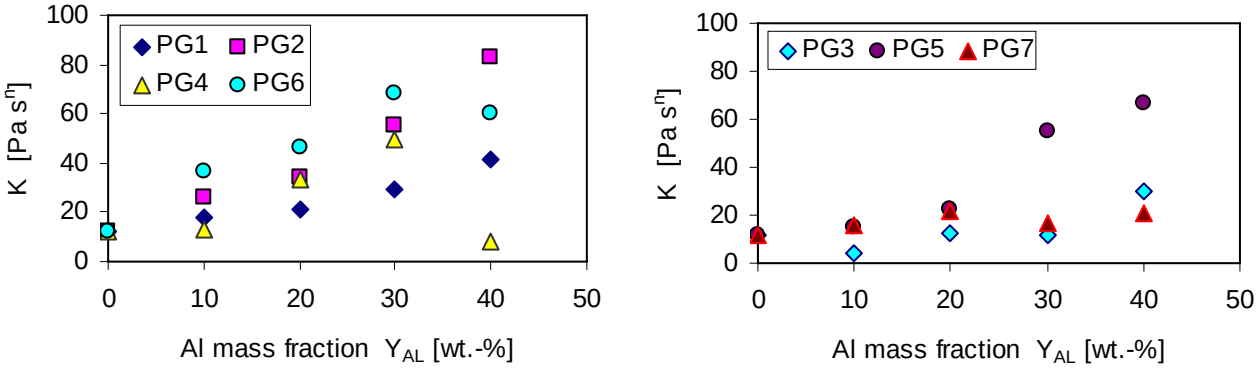


Figure 5: Pre-exponential factor *K* versus the Al mass fraction $Y_{Al}$ for gels with various Aluminium particle grades.

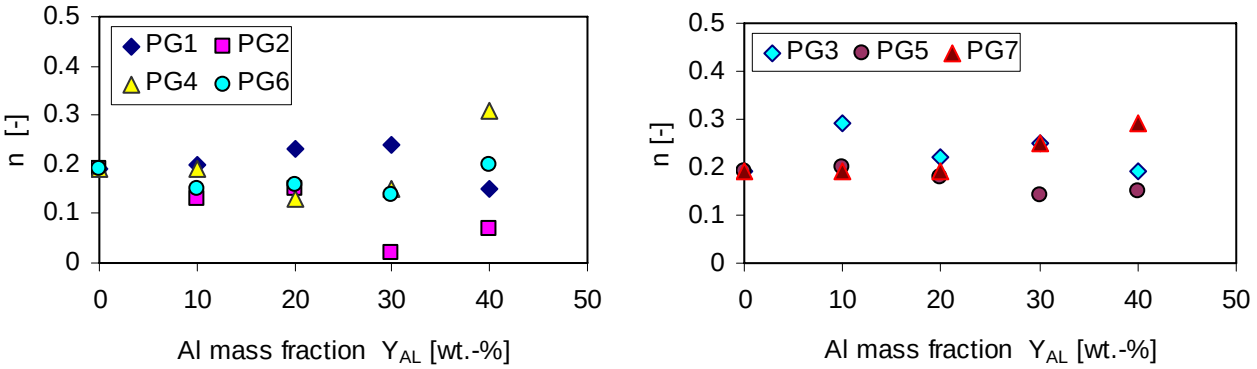


Figure 6: Exponential factor *n* versus the Al mass fraction $Y_{Al}$ for gels with various Aluminium particle grades.

Summarized it can be said that with increasing particle loading, increasing yield stresses $\tau_0$ and increasing *K* are determined. The exponent *n* does not vary significant for gels with low aluminium content. At particle loading of 30 % and higher, the HBE-parameter show generally higher irregularities than the gels with lower particle loadings.

### 3.2 Spray characteristics

For the spray investigations gels with the four particles grades PG1, PG2, PG5 and PG7 were produced to have a wide selection of particles sizes. Figure 7 presents typical shadowgraph images of the occurring spray regimes for the gels with the particle grade PG7 (Alpha Aesar, $D_{3,2}$=84.7 µm) in dependence of the average jet exit velocity $\bar{u}$. The HBE-generalized Reynolds number $Re_{gen\ HBE}$ was used to characterize the flow conditions in the injector. The number was introduced by Madlener et. al.[15] and its definition is given in Eq. 2.

$$\mathrm{Re}_{gen\,HBE} = \frac{\rho \cdot \bar{u}^{2-n} \cdot D^{n}}{\frac{\tau_0}{8}\left(\frac{D}{\bar{u}}\right)^{n} + K\left(\frac{3m+1}{4m}\right)^{n} 8^{n-1} + \eta_\infty \frac{3m+1}{4m}\left(\frac{D}{\bar{u}}\right)^{n-1}} \qquad \textbf{(2)}$$

$$with \quad m = \frac{n \cdot K\left(\frac{8\bar{u}}{D}\right)^{n} + \eta_\infty\left(\frac{8\bar{u}}{D}\right)}{\tau_0 + K\left(\frac{8\bar{u}}{D}\right)^{n} + \eta_\infty\left(\frac{8\bar{u}}{D}\right)}$$

The left pictures of each pair of shadowgraph images provide the view perpendicular to the plane spanned by the two gel jets, which is the observation direction of previous investigations; see e.g. Ref [4]. The parallel view to the liquid plane, obtained with the new experimental setup, is shown in the right pictures of the shadowgraph image sets.

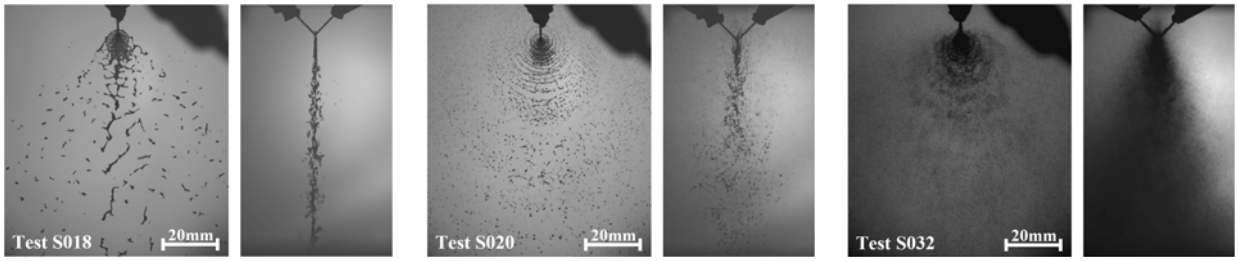


a) $\bar{u}$ = 3.9 m/s, $Re_{gen\ HBE}$ = 193 (Ray-shaped pattern)

b) $\bar{u}$ = 9.1 m/s, $Re_{gen\ HBE}$ = 697 (Ligament structures)

c) $\bar{u}$ = 58.5 m/s, $Re_{gen\ HBE}$ = 7772 (Fully developed pattern)

Figure 7: Shadowgraph images of a JetA-1/ThixatrolST-gel with 30 wt.-% Al particle PG7

Typical for all experimental conditions is that a fluid sheet is formed at the intersection point of both gel jets, which is orientated perpendicular to the plane created by the two gel jets. The shape of the sheet and the decay process are changing with increasing jet exit velocity $\bar{u}$. The different spray regimes were also discussed in previous publications[4] and are presented here in more detail due to the additional parallel observation direction. At low gel velocities $\bar{u}$ = 3.9 m/s (Fig. 7a) the fluid sheet shows ray-shaped structures on its surface and decays in ligaments, which move downstream preferred in direction of these surface "rays". On the side view image it can be seen that the separated ligaments are moving in a narrow area around the plane of the fluid sheet leading to a very small spray angle. This break-up mode was called ray-shaped pattern and was first observed with gels.[14]
At medium injector exit velocities $\bar{u}$ = 9.1 m/s, corresponding to the Reynolds number $Re_{genHBE}$ = 697 (Fig. 7b), circular, wave-like structures occur on the surface of the sheet and large bow-shaped ligaments are separated periodically from the rim. These ligaments decay downstream into smaller ones and droplets. This breakup mode is called ligament pattern. The side view shows a broader spray angle than for the ray-shaped pattern. At very high $Re_{genHBE}$ (Fig. 7c), the shape of the fluid sheet becomes small and irregular. It breaks up directly into very fine droplets without fragmenting into ligaments so that this breakup mode is called fully developed pattern. These droplets are preferably shed off in a periodic manner as waves from the sheet edge. On the side view it can be seen that a dense spray occurs with a broad spray angle.

Droplet size measurements of the spray were conducted with a Malvern droplet sizer for different gels at different injector exit velocities. Droplet sizes below 200 µm could be obtained for velocities higher than 15 m/s. In the left diagram of Fig. 8 the dependence of the Sauter mean diameter on the jet exit velocity $\bar{u}$ is presented for gelled fuels with various mass fractions $Y_{Al}$ of PG1 (Ecka, $D_{3,2}$=0.76 µm). For comparison also the measured droplet diameter of the liquid kerosene are included in the graph. It can be seen for all investigated fluids that with increasing injector

exit velocities $\bar{u}$ decreasing Sauter diameter $D_{3,2}$ occur, whereas the slope flattens for higher $\bar{u}$. At higher $\bar{u}$ a lower limit at about $D_{3,2} \approx 45$ µm seems to exist for all investigated fuels. The gel with 40 wt.-% aluminium shows a stronger irregularity, which seems to be caused by the higher Al loading of the gel.
In the right diagram of Fig. 8 the Sauter diameter is plotted in a logarithmic scale against the calculated HBE-generalized Reynolds number $Re_{genHBE}$ . The Reynolds numbers were calculated with Eq. 2 inserting the HBE-parameter and the density of the corresponding fluids. Due to its lower viscosity values, the liquid kerosene shows higher Reynolds numbers compared to the gelled fuels. The gradient of the presented curves, however, are similar. A similar characteristic could be obtained for the other investigated gels.

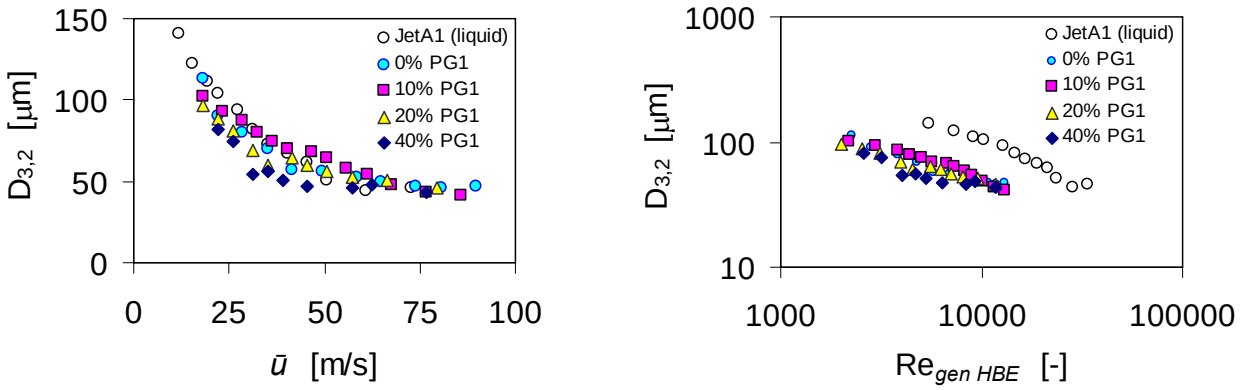


Figure 8: Average droplet diameter $D_{3,2}$ versus injector exit velocity $\bar{u}$ (left graph) and average droplet diameter versus HBE-generalized Reynolds number $Re_{genHBE}$ (right graph)

### 3.3 Combustion characteristics

Combustion experiments were conducted to investigate the combustion characteristics of metallised gels. Because for smaller average particle diameters higher combustion efficiencies can be expected, gels with the particle grade PG1 were chosen for the investigation. As a criterion for the quality of combustion, the efficiency ε was calculated. Heat losses through the combustion chamber wall were not considered. The efficiency is defined as the ratio of the real to the ideal difference between the outgoing and incoming heat fluxes. Based on the assumption that the specific heat capacities of the incoming air and fuel can be set to the specific heat capacity of the combustion gases (calculated with the Gordon McBride[19] program), the efficiency ε can be written according Eq. 3.

$$\varepsilon = \frac{\left|\dot{Q}_{out} - \dot{Q}_{in}\right|_{real}}{\left|\dot{Q}_{out} - \dot{Q}_{in}\right|_{ideal}} \approx \frac{T_{CC\,real} - T_{Air}}{T_{CC\,ideal} - T_{Air}} \qquad \textbf{(3)}$$

The real combustor temperature $T_{CC\,real}$ is calculated from the measured combustion pressure, the measured mass flows, the known area of the combustor exit and gas kinetic parameters. The ideal combustor temperature $T_{CC\,ideal}$ is calculated with the Gordon-McBride program for every conducted experiment based on the ideal combustion of the gel and the determined mass flows and pressures. The temperature of the incoming air flow $T_{Air}$ is measured directly at the entrance to the combustion chamber.
All combustion experiments were conducted at the same equivalence ratio $\phi = 0.23$. Combustion pressures were desired to be $p_{CC\,design}$ = 6 bar and 11 bar. Incoming air temperatures were desired to be $T_{Air\,design}$ =300 K, 550 K and 800 K. At these boundary conditions, the expected combustion temperatures $T_{CC\,design}$ could be calculated with Gordon-McBride for the different gel compositions.
Figure 9 shows the efficiency ε of the conducted experiments at a pressure level of 6 bar versus the determined real combustion temperatures $T_{CC\,real}$ . The dashed lines represent the theoretical distribution of the expected efficiencies for the desired combustion boundary conditions. The lines are limited for ε = 0 (no combustion) at $T_{CC\,real} = T_{Air\,design}$ and for ε = 1 (complete combustion) at $T_{CC\,real} = T_{CC\,design}$ . Due to the higher mass-related energy content of the aluminium, the combustion temperature $T_{CC\,design}$ increases with higher aluminium particle loadings. The symbols in Fig. 9 represent the calculated efficiencies for the conducted experiments. Only ideally the desired parameters (pressures, temperatures, mass flows, etc.) can be achieved by the experiments, therefore the symbols can show a slight deviation from the dashed lines representing the desired boundary conditions. The mass flow rate for the gelled

fuels was varied between ū = 30 m/s, 40 m/s, 50 m/s and 60 m/s. This choice was made because droplet diameters, derived from the spray experiments, were not adequate small below injector exit velocities ū < 25 m/s. Due to limits in the air supply of the test bench some desired working conditions could not be realized.
Since the symbols of the conducted experiments in Fig. 9 are situated on their corresponding dashed lines, it shows that the desired working conditions were mostly achieved by the experiments. The obtained values for the efficiency are up to 53%. Heat losses through the combustion are not considered. It could mostly be obtained, that higher mass flow rates of fuel lead to higher efficiencies. It is assumed that this is caused by the smaller droplets created by the spray conditions according Fig. 8.
Figure 10 shows the efficiencies of the conducted combustion experiments at the higher pressure level of 11 bar. It can be seen, that the values of ε are generally higher compared to the ε for the lower pressure level in Fig. 9. Again, increasing efficiencies were measured with increasing injector exit velocities of the gelled fuels.

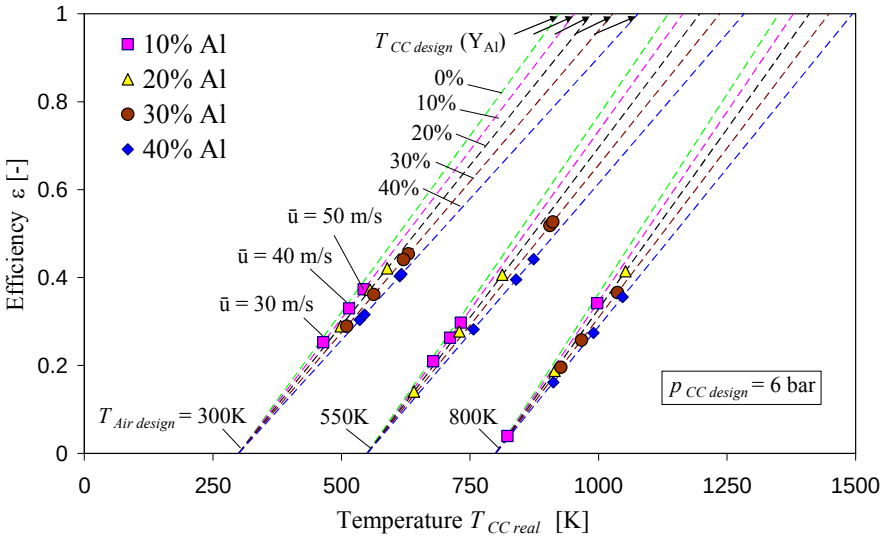


Figure 9: Combustion efficiency ε vs. real combustor temperature $T_{CC\,real}$ for 4 different aluminium mass fractions of PG1 and 3 different air heater temperatures $T_{Air}$ at a pressure level of $p_{CC\,design}$ = 6 bar

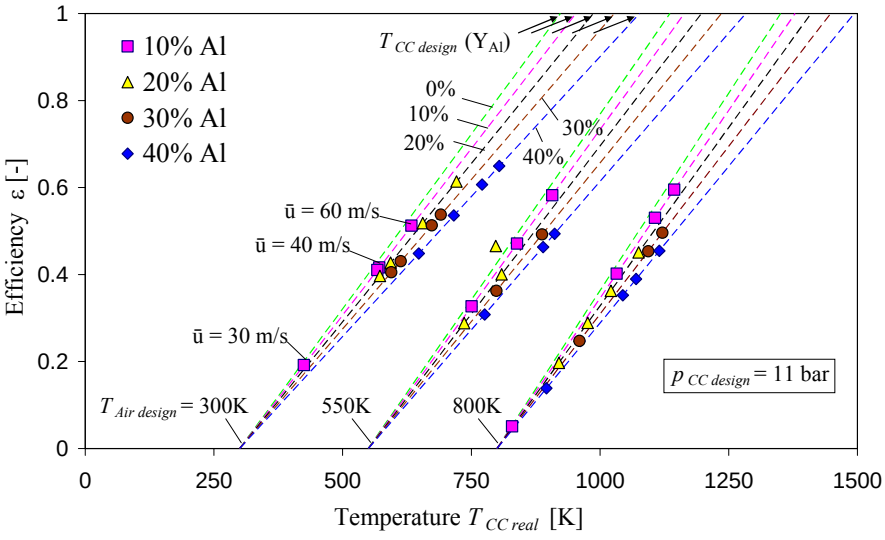


Figure 10: Combustion efficiency ε vs. real combustor temperature $T_{CC\,real}$ for 4 different aluminium mass fractions of PG1 and 3 different air heater temperatures $T_{Air}$ at a pressure level of $p_{CC\,design}$ = 11 bar

As a summary of the combustion characteristic, Figure 11 shows the calculated efficiency $\bar{\varepsilon}$ for the different pressure levels and particle loadings as an average of all conducted mass flow rates see. At the low pressure level it

can be seen, that the average efficiency of the combustion reaches a maximum for the gel containing 30 wt.-% of aluminium. At the higher pressure level of 11 bar this characteristic was obtained less pronounced.

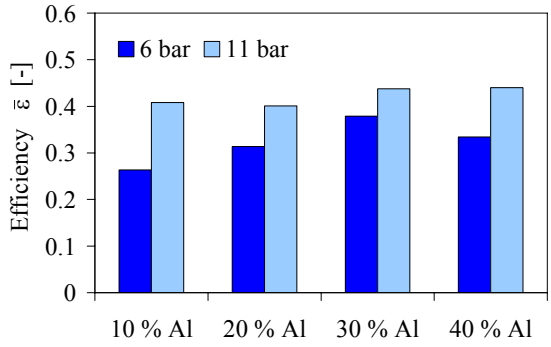


Figure 11: Mean efficiencies $\bar{\varepsilon}$ of the gels with four different particle loadings at the two different pressure levels

## 4. Conclusions

A detailed investigation concerning the influence of various parameters like average particle diameter and mass content on the rheological, spray and combustion characteristics of Al-particle loaded gelled fuels was conducted. The rheological measurements of gels with 7 different particle grades with average particle diameters $D_{3,2}$ in the range between 0.76 µm and 84.75 µm, showed increasing yield stresses with increasing aluminium mass fraction. The experimentally determined viscosity characteristic was approached with the theoretical Herschel-Bulkley-Extended viscosity law, whose corresponding parameters where presented.
For the subsequently conducted spray investigations with a doublet like-on-like impinging jet injector setup, gels with four different aluminium particle grades were selected. By taking shadowgraph images, fully developed spray patterns were observed for high injector exit velocities. Droplet size measurements showed that with increasing gel jet velocities decreasing droplet diameters occur. All gels showed an asymptotic value of about $D_{3,2} \approx 45$ µm for the droplet diameters at high exit velocities. Summarizing it can be said that the measured viscosity and also the measured droplet diameters of the investigated gels are within a distinct bandwidth. Thus the aluminized gel with the smallest particle grade ($D_{3,2}$=0.76 µm) was chosen for the combustion experiments, so that high combustion efficiencies within the combustor could be expected. The determination of the combustion efficiency at 6 and 11 bar combustor pressure level under ramjet relevant conditions showed increasing efficiencies with increasing combustor pressure and generally increasing efficiencies with increasing jet exit velocity. A maximum efficiency could be obtained for the gel with 30 wt.-% of aluminium particle loading.

## Acknowledgements

The help of A. Feinauer during the running of the tests and of R. Brändle during the production of the gel fuels is kindly acknowledged. Also the discussions, comments and proposals of Prof. L. DeLuca have been a great help for the conduction of the work. Furthermore we would like to thank Dr. K. Menke and his colleagues from the Fraunhofer Institute for Chemical Technology in Pfinztal for the determination of the average Al particle diameters.

## Nomenclature

| | |
|---|---|
| $D_{3,2}$ | average droplet diameter (Sauter mean), m |
| $D_{50}$ | average droplet diameter (50%), m |
| $D_5$ | particle diameter at 5%, m |
| $D_{95}$ | particle diameter at 95%, m |
| D | injector orifice diameter, m |
| $K$ | pre-exponential factor, Pa $s^n$ |
| $n$ | exponential factor, - |
| Re | Reynolds number, - |
| s | slenderness ratio, - |
| T | temperature, K |
| $\bar{u}$ | jet exit velocity, m/s |
| $Y_{Al}$ | mass fraction of aluminium, - |

*Greek letters*

| | |
|---|---|
| $\dot{\gamma}$ | shear rate, 1/s |
| $\Delta d$ | diameter width, m |
| $\varepsilon$ | combustion efficiency, - |
| $\bar{\varepsilon}$ | average combustion efficiency, - |
| $\Phi$ | equivalence ratio, - |
| $\theta$ | impingement half angle, -° |
| $\eta$ | dynamic shear viscosity, Pa·s |
| $\eta_\infty$ | viscosity of upper Newtonian plateau, Pa·s |
| $\tau_0$ | yield stress, Pa |

*Subscripts and abbreviations*

| | |
|---|---|
| Al | aluminium |
| CC | combustion chamber |
| gen | generalized |
| HBE | Herschel-Bulkley-Extended |

## References


[1] Schindler, R.C., Olson, A.M. and Arnold, C.J. A gelled propellant sustainer stage. AIAA-Paper 92-1122, *AIAA Aerospace Design Conference*, Irvine, CA, USA, February 1992.

[2] Natan, B. and Rahimi, S. The status of gel propellants in year 2000. In: Combustion of Energetic Materials (Eds.: K.K. Kuo and L.T. DeLuca), Begell House, New York, 2002, pages 172-194.

[3] Ciezki, H.K., Bartels, N., von Kampen, J. and Madlener, K. Properties of gelled propellants for throttleable propulsion systems. *Symposium on Energy Conversion Fundamental*, Istanbul, Turkey, 21-23 June 2004.

[4] von Kampen, J., Alberio, F. and Ciezki, H.K. Spray and combustion characteristics of aluminized gelled fuels with an impinging jet injector. *Aerospace Science and Technology*, 11:77–83, 2007 and *EUCASS*, Moscow, July 2005

[5] Nachmoni, G. and Natan, B. Combustion characteristics of gel fuels. *Combustion Science and Technology*, 156:139-157, 2000.

[6] Szekely Jr., G.A. and Faeth, G.M. Combustion properties of carbon slurry drops, *AIAA Journal*, 20:3:422-429, 1982.

[7] Lee, A. and Law, C.K. Gasification and shell characteristics in slurry droplet burning. *Combustion and Flame*, 85:85-93, 1991.

[8] Mueller, D.C. and Turns, S.R. Some aspects of secondary atomization of aluminum/hydrocarbon slurry propellants, *Journal of Propulsion and Power*, 9:3:345-352, 1993.

[9] Ciezki, H.K. and, Natan, B. An Overview of Investigations on Gel Fuels for Ramjet Applications," ISABE 2005-1065, *ISABE2005, 17th Int. Symposium on Airbreathing Engines*, Munich, Germany, 4-9 September 2005.

[10] Kampen, J., Madlener, K. and Ciezki, H.K. Characteristic flow and spray properties of gelled fuels with regard to the impinging jet injector type. AIAA-2006–4573, *42nd AIAA Joint Propulsion Conference*, Sacramento, CA, USA, 9-12 July 2006.

[11] Sutton, G.P. Rocket propulsion element: an introduction to the engineering of rockets. John Whiley, New York, USA, pages 298-311, 1992.

[12] Madlener, K., Moser, H.A. and Ciezki, H.K. Influence of the injector inlet angle on the flow and spray behavior of shear thinning fluids in impinging jet injectors. *38th Int. Annual Conference of ICT*, Karlsruhe, Germany, 26-29 June 2007.

[13] Madlener, K. and Ciezki, H.K. Analytical description of the flow behavior of extended Herschel Bulkley fluids with regard to gel propellants. *36th Int. Annual Conference of ICT & 32nd Int. Pyrotechnics Seminar*, Karlsruhe, Germany, 28th June – 1st July 2005, pp. 186/1 – 186/13.

[14] N. Bartels, J. von Kampen, H.K. Ciezki, N. Zanetti, Investigation of the spray characteristic of an aluminized gelled fuel with an impinging jet injector. *Proc 35th Annual Conference of ICT*, Karlsruhe, Germany, June 2004.

[15] Madlener, K., Frey, B. and Ciezki, H.K. Generalized Reynolds number for non-Newtonian fluids. *EUCASS-2007*, 2-6 July 2007, Brussels, Belgium.

[16] Metzner, A.B. and Reed, J.C. Flow of non-Newtonian fluids - correlation of the laminar, transition, and turbulent-flow regions. *A.I.Ch.E. Journal B1*, 1:4:434-440, 1955.

[17] Dodge, D.W. and Metzner, A.B. Turbulent flow of non-Newtonian systems. *A.I.Ch.E. Journal*, 5:2:189-204, 1959.

[18] Ryan, N.W. and Johnson, M.N. Transition from laminar to turbulent flow in pipes. *A.I.Ch.E. Journal*, 5:2: 433-438, 1959.

[19] McBride, B.J. and Gordon, S. Computer program for calculation of complex chemical equilibrium compositions and applications. Part II. NASA Reference Publication 1311, June 1996.

This page has been purposedly left blank